NATURAL CONVECTION HEAT AND MOMENTUM TRANSFER IN SQUARE CAVITIES DISCRETELY HEATED FROM BELOW AND COOLED FROM ABOVE AND ONE SIDE

C. Cianfrini, M. Corcione, E. Habib*, A. Quintino
*Author for correspondence
DIAEE – Sezione Fisica Tecnica, Sapienza
Sapienza University of Rome,
via Eudossiana 18, Roma, 00184,
Italy,
E-mail: emanuele.habib@uniroma1.it

ABSTRACT

Laminar natural convection heat transfer inside rectangular enclosures partially heated from below and cooled at the top and one side, filled with either a gas or a liquid, is studied numerically. A specifically developed computer-code based on the SIMPLE-C algorithm is implemented for solving the coupled system of mass, momentum, and energy conservation equations. Numerical simulations are performed for representative combinations of (a) the heated fraction of the bottom wall, sweeping from 0.2 to 0.8, (b) the Rayleigh number based on the cavity width, ranging from 10^2 to 10^7, and (c) the Prandtl number, spanning from 0.7 to 700. Resorting on computed velocity and temperature fields, all possible heat transfer avenues are explored and analyzed in detail. It is found that the amount of heat transferred across the enclosure increases with increments in the Rayleigh number and/or the Prandtl number and/or the size of the heater. Dimensionless heat transfer correlating equations are developed for purposes of engineering design.

INTRODUCTION

Natural convection inside rectangular enclosures has been extensively studied both experimentally and numerically, owing to its importance in many engineering applications, e.g., heat transfer in buildings, solar energy collection, heat removal in micro-electronics, and cooling of nuclear reactors, to name a few.

Most of the papers on this topic are related to unidirectional heat flows, as pointed out by Ostrach [1] and Bejan [2], but real-life systems are more usually characterized by multidirectional heat flows, i.e., neither simply horizontal or vertical. Moreover, in many practical cases mixed thermal conditions on the same boundary wall may also be encountered, which is, e.g., what happens when a boundary wall is only partially heated or cooled. Focusing the interest on the heating-from-below situation several studies on this topic are readily available in the specialized literature [3-12]. Other investigations were also conducted to study the influence of the fluid on the natural convection performances in square and rectangular cavities [13-14].

In this background, the aim of the present paper is to carry out a study on natural convection heat and momentum transfer inside square cavities, partially heated at the bottom, and cooled at the top and one sidewall, using fluids with Prandtl number spanning from 0.7 to 700. In particular, the heater, which is placed in the middle of the bottom endwall, is assumed to be kept at uniform temperature. The remainder of the bottom wall and the other sidewall are assumed to be perfectly insulated.
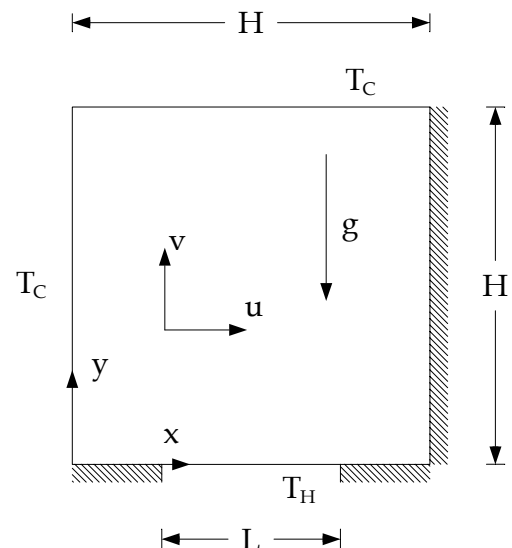

Figure 1 Sketch of the geometry and coordinate system

NOMENCLATURE

E	[-]	Dimensionless size of the heater
g	[m^2/s]	Gravity vector
g	[m^2/s]	Gravitational acceleration
H	[m]	Height of the enclosure
h	[W/m^{2}K]	Average coefficient of convection
k	[W/m K]	Thermal conductivity of the fluid
L	[m]	Length of the heater
Nu	[-]	Average Nusselt number based on $H = hH/k$
Nu^*	[-]	Average Nusselt number based on $L = hL/k$
P	[-]	Dimensionless pressure
p	[Pa]	pressure
Pr	[-]	Prandtl number $= \nu/\alpha$
Q	[W/m]	Heat transfer rate per unit length
Ra	[-]	Rayleigh number based on $H = g\beta(t_H - t_C)H^3Pr/\nu^2$
Ra_L	[-]	Rayleigh number based on $L = g\beta(t_H - t_C)L^3Pr/\nu^2$
T	[-]	Dimensionless temperature
t	[K]	Temperature
U	[-]	X-wise dimensionless velocity component
V	[-]	Dimensionless velocity vector
V	[-]	Y-wise dimensionless velocity component
X,Y	[-]	Dimensionless Cartesian coordinates

Greek symbols

α	[m^2/s]	Thermal diffusivity of the fluid
β	[1/K]	Coefficient of volumetric thermal expansion of the fluid
ν	[m^2/s]	Kinematic viscosity of the fluid
ρ	[kg/m^3]	Density of the fluid
τ	[-]	Dimensionless time
Ψ	[-]	Dimensionless stream function

Subscripts

C	Cold
H	Hot
in	Ingoing
max	Maximum value
put	Outgoing

MATHEMATICAL FORMULATION

A square enclosure of height H is partially heated at the bottom, and cooled at the top and one sidewall. The middle portion of the bottom wall, of length L, is heated at uniform temperature t_H, while the cooled walls are kept uniform temperature t_C. The remainder of the bottom wall, as well as the other sidewall, are considered adiabatic, as sketched in Fig. 1, where the coordinate system adopted is also represented.

The flow is assumed to be two-dimensional, laminar and incompressible, with constant fluid properties and negligible viscous dissipation and pressure work. The buoyancy effects on momentum transfer are taken into account through the customary Boussinesq approximation.

Once the above assumptions are employed in the conservation equations of mass, momentum and energy, the following set of governing equations is obtained:

$$\nabla \cdot \mathbf{V} = 0 \tag{1}$$

$$\frac{\partial \mathbf{V}}{\partial \tau} + (V \cdot \nabla)\mathbf{V} = -\nabla P + \nabla^2 \mathbf{V} - \frac{Ra}{Pr}T\frac{\mathbf{g}}{g} \tag{2}$$

$$\frac{\partial T}{\partial \tau} + (\mathbf{V} \cdot \nabla)T = \frac{1}{Pr}\nabla^2 T \tag{3}$$

where **V** is the velocity vector having dimensionless velocity components U and V normalized by ν/H, T is the dimensionless temperature excess over the uniform temperature of the cooled sidewall normalized by the temperature difference $(t_H - t_C)$, τ is the dimensionless time normalized by H^2/ν, P is the dimensionless pressure normalized by $\rho\nu^2/H^2$, **g** is the gravity vector, $Pr = \nu/\alpha$ is the Prandtl number, and Ra is the Rayleigh number defined as:

$$Ra = \frac{g\beta(t_H - t_C)H^3}{\alpha\nu} \tag{4}$$

The other parameter which enter into this study is the dimensionless size of the heater:

$$E = \frac{L}{H} \qquad 0.2 \leq E \leq 0.8 \tag{5}$$

The boundary conditions assumed are: (a) T =1 and **V** = 0 at the heated surface; (b) T = 0 and **V** = 0 at the cooled surface; and (c) $\partial T/\partial n = 0$ and **V** = 0 at the adiabatic surfaces, where n denotes the normal to the surface.

The initial conditions assumed are fluid at rest, i.e., **V** = 0, and uniform temperature T = 0 throughout the whole cavity.

COMPUTATIONAL PROCEDURE

The set of governing equations (1)-(3) with the boundary conditions stated above is solved through a control-volume formulation of the finite-difference method. The pressure-velocity coupling is handled by the SIMPLE-C algorithm introduced by Van Doormaal and Raithby [15], which is essentially a more implicit variant of the SIMPLE algorithm developed by Patankar and Spalding [16]. The QUICK discretization scheme proposed by Leonard [17] is used for the evaluation of the interface fluxes. A second-order backward scheme is used for time stepping. Starting from the assigned initial fields of the dependent variables across the cavity, at each time-step the discretized governing equations are solved iteratively through a line-by-line application of the Thomas algorithm, enforcing under-relaxation to ensure convergence. Details on the SIMPLE procedure, as well as on enhanced variants of the basic algorithm, may be found in Patankar [18, 19].

The computational spatial domain is covered with a nonuniform grid, having a higher concentration of grid lines near the boundary walls and both ends of the heat source, and a uniform spacing throughout the remainder interior of the cavity. Time discretization is chosen uniform. Within each time-step, the spatial solution is considered to be converged when the maximum absolute values of both the mass source and the relative changes of the dependent variables at any grid-node from iteration to iteration are smaller than the prescribed values, i.e., 10^{-4} and 10^{-5} respectively. Time-integration is

stopped once steady-state is reached. This means that the simulation procedure ends when the relative difference between the incoming and outgoing heat transfer rates, and the relative changes of the time-derivatives of the dependent variables at any grid-node between two consecutive time-steps, are smaller than the pre-set values, i.e., 10^{-6} and 10^{-7}, respectively. Actually, a limited number of configurations related to high Prandtl and Rayleigh numbers are featured by unsteady non-periodic solutions, as it will be discussed later in more detail.

After convergence is attained, the average Nusselt numbers Nu_H and Nu_C of the heated and cooled boundaries, respectively, are calculated:

$$Nu_H = \frac{h_H H}{k} = \frac{Q_{in} H}{kL(t_H - t_C)} =$$
$$= \frac{1}{E} \cdot \frac{Q_{in}}{k(t_H - t_C)} = \qquad (6)$$
$$= -\frac{1}{E} \int_{(1-E)/2}^{(1+E)/2} \left. \frac{\partial T}{\partial Y} \right|_{Y=0} dX$$

$$Nu_C = \frac{h_C H}{k} = \frac{Q_{out} H}{2kH(t_C - t_H)} =$$
$$= \frac{1}{2} \cdot \frac{Q_{out}}{k(t_C - t_H)} = \qquad (7)$$
$$= \frac{1}{2} \int_0^1 \left. \frac{\partial T}{\partial X} \right|_{X=0} dY - \frac{1}{2} \int_0^1 \left. \frac{\partial T}{\partial Y} \right|_{Y=1} dX$$

where h_H and h_C are the average coefficients of convection of the heated and cooled boundary surfaces, respectively, and Q_{in} and Q_{out} are the overall incoming and outgoing heat transfer rates, respectively. The temperature gradients at any boundary surface are evaluated through a second-order profile among each wall-node and the next corresponding two fluid-nodes. Of course, since at steady-state the incoming and outgoing heat transfer rates must be the same, i.e., $Q_{in} = -Q_{out} = Q$, in all the steady-state solutions the following relationship between Nu_H and Nu_C holds:

$$\frac{Nu_H}{Nu_C} = \frac{2}{E}$$

Tests on the dependence of the results on both grid-size and time-step have been performed for several combinations of the independent variables E, Pr and Ra. The optimal grid-size and time-step used for computations, which represent a good compromise between solution accuracy and computational time, are such that further refinements do not yield for noticeable modifications neither in the temperature nor in the flow field. Typically, the number of nodal points lies in the range between 30×30 and 80×80, and the time stepping lie in the range between 10^{-3} and 10^{-6}. Full details on the code validation are discussed in [20].

RESULTS AND DISCUSSION

Numerical simulations are performed for different values of (a) the dimensionless size of the heater E in the range between 0.2 and 0.8, (b) the Rayleigh number Ra in the range between 10^2 and 10^7, and (c) the Prandtl number Pr in the range between 0.7and 700.

A selection of local results is presented in Figs. 2 to 7, where isotherm contours are plotted for different sets of values of E, Ra and Pr, in order to highlight the effects of any independent variables on the temperature and flow fields. In the isotherm plots, the contour lines correspond to equispaced values of the dimensionless temperature T in the range between 0 and 1. In the streamline plots, the contour lines correspond to equispaced values of the normalized dimensionless stream function $|\Psi|/|\Psi|_{max}$ in the range between 0 and 1, where Ψ is defined as usual by $U = \partial\Psi/\partial Y$ and $V = -\partial\Psi/\partial X$.

As expected, the flow field consists of a rotating cell, that moves downwards along the cooled sidewall and rises along the opposite sidewall after being heated in the middle of the bottom wall. The intensity of the fluid motion, which depends on the relative importance of the buoyancy driving force and the viscous force: (a) increases as the heated fraction of the bottom wall increases, which may be derived by comparing Figs. 2, 3, and 4; (b) increases as the Rayleigh number Ra increases, which is evident in Figs. 5, 6, and 7; (c) decreases as the Prandtl number Pr increases, although it slightly affects the overall heat transfer performances.

For thick liquids, at high Rayleigh number, i.e. $10^6 - 10^7$, the low pattern changes into a two superimposed counter-rotating cells, as highlighted by the streamline plots in Figs. 8 and 9. These configurations, whose solutions at a given time are delineated by dashed lines, are not steady, with non-periodic cyclic fluctuations , as shown in Fig. 10, where six snapshots taken at same $\Delta\tau = 0.02$ are reported, for E = 0.8, Ra = 10^6, and Pr = 7.

The local Nusselt number ($Nu_H(X) = -\frac{\partial T}{\partial Y}$) along the heater is higher toward the cold sidewall, decreasing very steeply as one moves towards the adiabatic sidewall, as shown in Fig. 11 for Pr = 7, E = 0.6 and Ra = 10^3 to 10^6, and Fig. 12 for Ra = 10^5, E = 0.6 and Pr = 0.7 to 700.

As far as the overall results are concerned, the heat transfer performance of the whole cavity is expressed in terms of Nu_C, which is considered more appropriate to this purpose than Nu_H. In fact, as said above, once Ra is assigned, the amount Q of heat transferred across the enclosure increases with increasing the heated fraction E of the bottom endwall. Correspondingly, a Nusselt number which would represent the thermal behavior of the cavity "at a glance" should increase with increasing E. On the other hand, according to eq. (6), it is $Nu_H \sim Q/E$. This means that Nu_H may either increase or decrease with E, depending on whether $\partial Q/\partial E$ is positive or negative. In contrast, according to eq. (7), $Nu_C \sim Q$, which implies that Nu_C unequivocally increases with E. For this same reason, the effectiveness of heat removal from the bottom surface is described through an alternative Nusselt number Nu* which uses L instead of H as characteristic length:
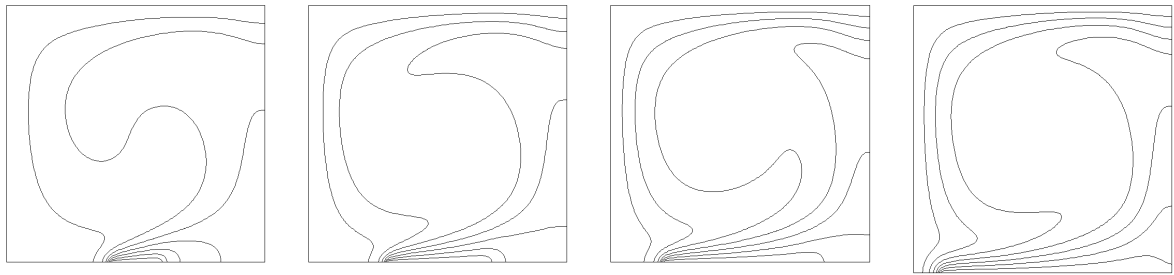
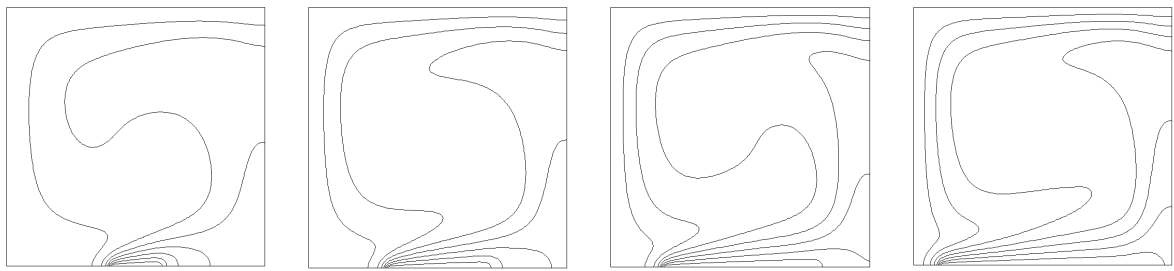**Figure 2** Isotherms for Ra = 10^5, Pr = 0.7 and E = 0.2, 0.4, 0.6, 0.8

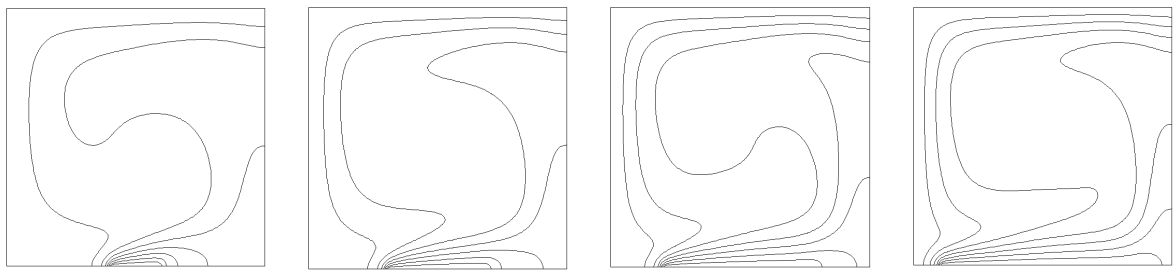**Figure 3** Isotherms for Ra = 10^5, Pr = 7 and E = 0.2, 0.4, 0.6, 0.8

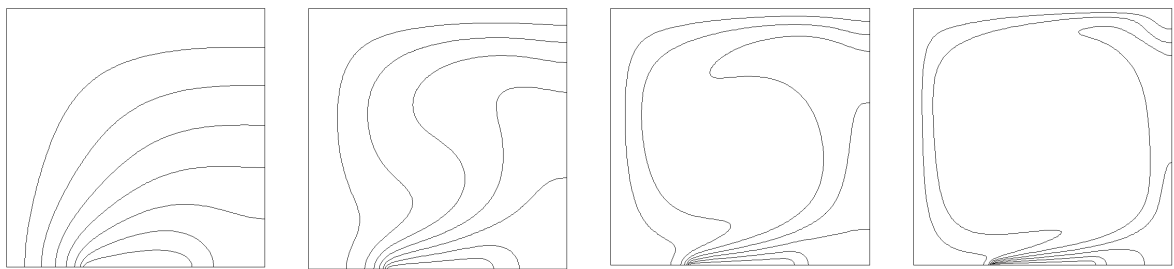**Figure 4** Isotherms for Ra = 10^5, Pr = 700 and E = 0.2, 0.4, 0.6, 0.8

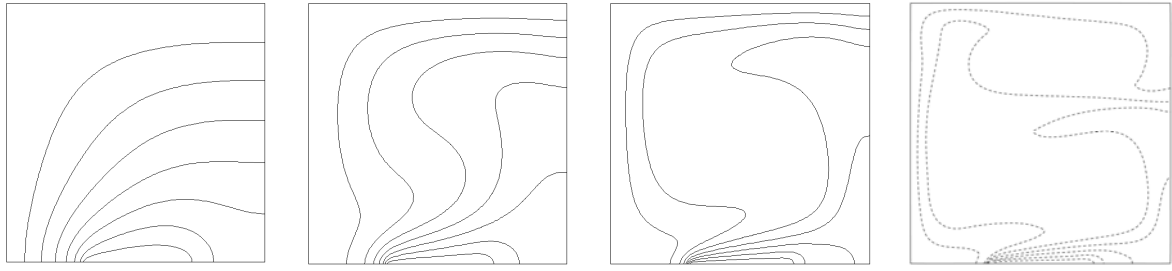**Figure 5** Isotherms for Pr = 0.7, E = 0.4 and Ra = 10^3, 10^4, 10^5, 10^6

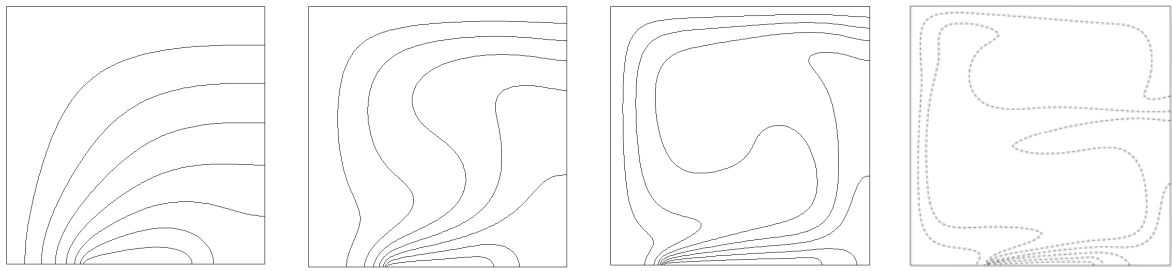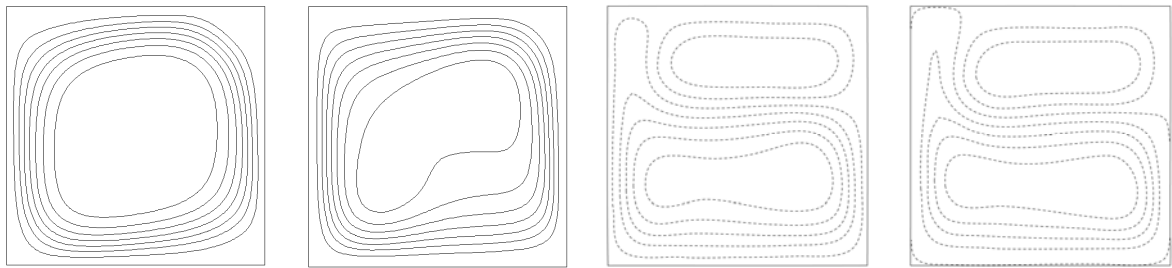**Figure 6** Isotherms for Pr = 7, E = 0.4 and Ra = 10^3, 10^4, 10^5,10^6

Figure 7 Isotherms for Pr = 700, E = 0.4 and Ra = 10^3, 10^4, 10^5,10^6

Figure 8 Streamlines for E = 0.4, Ra = 10^6 and Pr = 0.7, 2, 7, 700
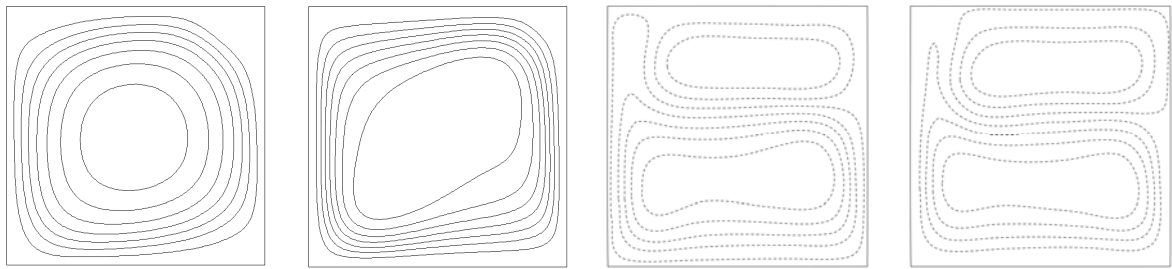

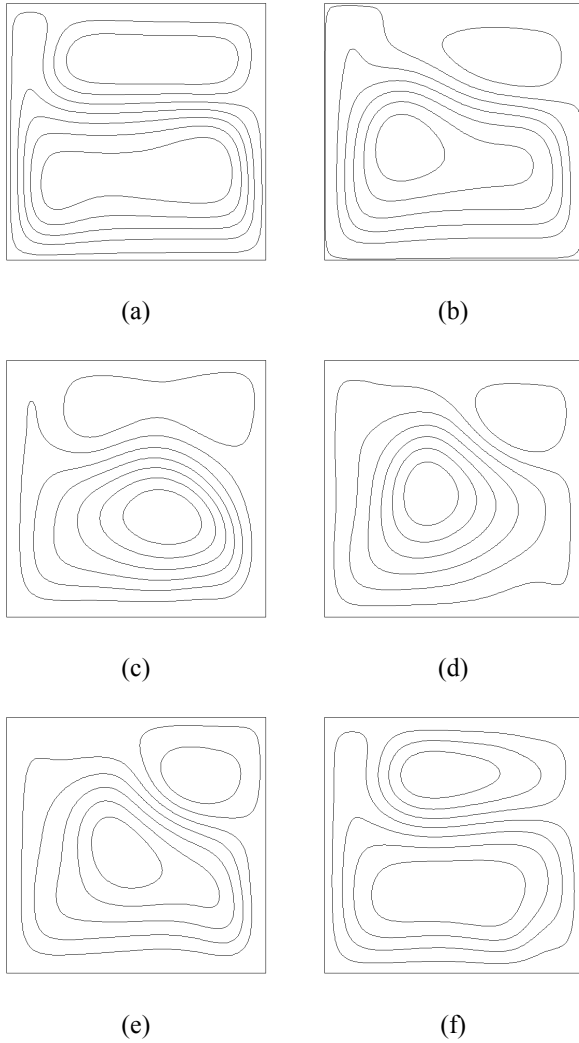**Figure 9** Streamlines for E = 0.8, Ra = 10^6 and Pr = 0.7, 2, 7, 700

(a)　　　　　　　(b)

(c)　　　　　　　(d)

(e)　　　　　　　(f)

Figure 10 Stremlines for Pr = 7, E = 0.8 and Ra = 10^6 showing the time evolution of the flow pattern ($\Delta\tau = 0.02$)

$$Nu^* = \frac{h_H L}{k} = \frac{Q_{in} L}{kL(t_H - t_C)} = E\,Nu_H = 2Nu_C \qquad (8)$$

Distributions of Nu* vs. Ra are plotted in Fig. 13 for Pr = 7 and E = 0.2 to 0.8 and in Fig. 14 for E = 0.8 and Pr = 0.7 to 700, where for the unsteady heat transfer configurations the time averaged values of Nu* (over a period long enough so that for any further increase of the integration period the percent change would be less than 10^{-3}) are depicted in full symbols.

As regards the development of a correlation among Nu* and the independent variables E, Ra and Pr, the Rayleigh number Ra_L based on the length L of the heated portion of the bottom end is introduced:

$$Ra_L = \frac{g\beta(t_H - t_C)L^3}{\nu^2} Pr \qquad (9)$$

In fact, on account of eqs. (4)-(5) and (9), the following relationship holds:

$$Ra_L = Ra\,E^3 \quad (10)$$

Therefore, Ra_L increases with Ra and E, which is exactly what happens for the heat transfer rate across the cavity, as discussed earlier, thus implying that Ra_L can be used for a more synthetic first-approach "description" of the problem treated here.
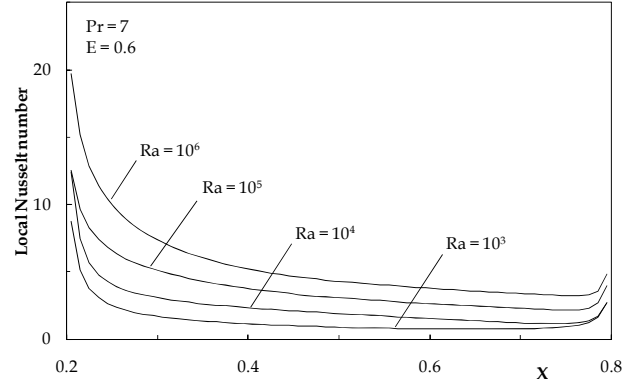

Figure 11 Distributions of the local Nusselt number along the heater for Pr = 7, E = 0.6 and different values of Ra
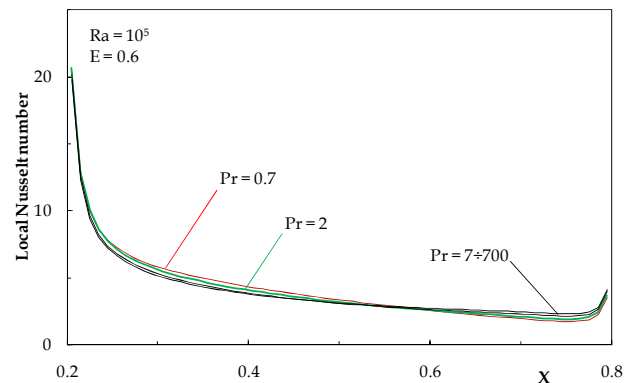

Figure 12 Distributions of the local Nusselt number along the heater for Ra = 10^5, E = 0.6 and different values of Pr
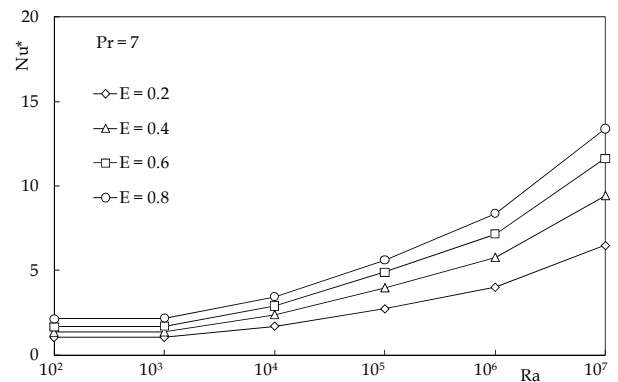

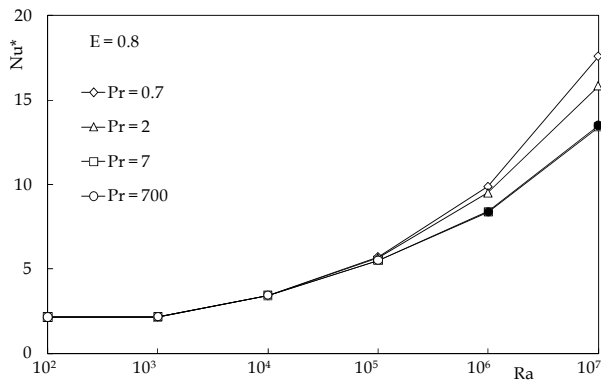**Figure 13** Distributions of Nu* vs. Ra for Pr = 7 and different values of the heater size E

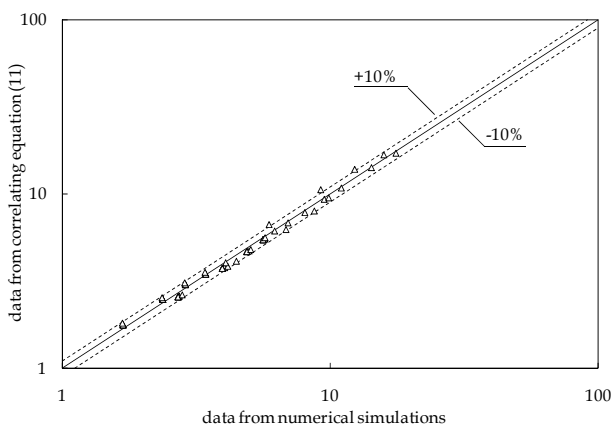**Figure 14** Distributions of Nu* vs. Ra for E = 0.8 and different values of the Prandtl number Pr

Figure 15 Comparison between Nu* from eq. (19) and Nu* from numerical simulations

Indeed, the numerical results obtained for Nu*, and then for $Nu_C = 0.5 \ Nu*$, can be expressed by the following correlating equation:

$$Nu* = A\left(\frac{Ra_L \ Pr}{Pr - 0.1}\right)^b \qquad (11)$$

where

$$A = -0.11 \cdot \log(Ra) + 1.31 \qquad (12)$$

$$b = 0.02 \cdot \log(Ra) + 0.082 \qquad (13)$$

for $0.2 \leq E \leq 0.8$, $0.7 \leq Pr \leq 700$, and $10^4 \leq Ra \leq 10^7$, with a 5.39% standard deviation of error, and a ±10% range of error with a 96% level of confidence, as shown in Fig. 15.

CONCLUSIONS

Natural convection inside square enclosures, filled with both liquids and gases, discretely heated at the bottom and cooled from above and one side, has been studied numerically,

for different values of the heater size, the Rayleigh number, and the Prandtl number.

It has been found that, as long as the flow field is steady, the flow structure is a single cell. At high Rayleigh numbers in thick liquids, an unsteady non-periodic counter-rotating cell appears just under the cold upper endwall. The intensity of the fluid motion, and then the consequent heat transfer rate across the enclosure, increases with increasing the heater size and the Rayleigh number, and decreases with increasing the Prandtl number, although it has little influence on the heat transfer performances.

Finally, the effectiveness of heat removal from the partially heated bottom wall is described better through a Nusselt number based on the length of the heater.

REFERENCES

[1] S. Ostrach, Natural convection in enclosure, J. Heat Transfer, 110 (1988) 1175-1190.

[2] A. Bejan, Convection Heat Transfer, New York, Wiley, 1982.

[3] I. Sezai and A.A. Mohamad, Natural convection from a discrete heat source on the bottom of a horizontal enclosure, Int. J. Heat Mass Transfer 43 (2000) 2257-2266.

[4] O. Aydin and W.-J. Yang, Natural convection in enclosures with localized heating from below and symmetrical cooling from sides, Int. J. Num. Meth. Heat Fluid Flow 10 (2000) 518-529.

[5] Q.-H. Deng, G.-F. Tang and Y. Li, A combined temperature scale for analyzing natural convection in rectangular enclosures with discrete wall heat sources, Int. J. Heat Mass Transfer 45 (2002) 3437-3446.

[6] B. Calcagni, F. Marsili and M. Paroncini, Natural convective heat transfer in square enclosures heated from below, Applied Thermal Engineering 25 (2005) 2522-2531.

[7] P.H. Oosthuizen and J.T. Paul, Natural convection in a rectangular enclosure with two heated sections on the lower surface, Int. J. Heat Fluid Flow 26 (2005) 587-596.

[8] T. Basak, S. Roy, A.R: Balakrishnan, Effects of thermal boundary conditions on natural convection flows within a square cavity, Int. J. Heat Mass Transfer 49 (2006) 4525-4535

[9] N.B. Cheikh, B. Ben Beya, T. Lili, Influence of thermal boundary conditions on natural convection in a square enclosure partially heated from below, Int. Comm. Heat Mass Transf. 34 (2007) 369-379

[10] T.Z. Chen, L.Y. Chen, Study of bouyancy-induced flows subjected to partially heated sources on the left and bottom walls in a square enclosure, Int. J. Therm. Sci 46 (2007) 1219-1231

[11] S. Bnerjee, A. Mukhopadhyay, S. Sen, R. Ganguly, Natural convection in a bi-heater configuration of passive electronic cooling, Int. J. Therm. Sci. 47 (2008) 1516-1527

[12] S. Saravanan, C. Sivaraj, Natural convection in an enclosure with a localized nonuniform heat source on the bottom wall, Int. J. Heat Mass Transfer 54 (2011) 2820-2828

[13] O. Turan, A. Sachdeva, N. Chakraborty, R.J. Poole, Laminar natural convection of power-law fluids in a square enclosure with differenially heated side walls subject to constant temperatures, Journal of Non-Newtonian Fluid Mechanics 166 (2011) 1049–1063

[14] O. Turan, R.J. Poole, N. Chakraborty, Influences of boundary conditions on laminar natural convection in rectangular enclosures with differentially heated side walls, Int. J. Heat Fluid Flow 33 (2012) 131-146

[15] J.P. Van Doormaal and G.D. Raithby, Enhancements of the simple method for predicting incompressible fluid flows, Numer. Heat Transfer 11 (1984) 147-163.

[16] S. V. Patankar and D. B. Spalding, A calculation procedure for heat, mass and momentum transfer in three-dimensional parabolic flows, Int. J. Heat Mass Transfer 15 (1972) 1787-1797.

[17] B. P. Leonard, A stable and accurate convective modelling procedure based on quadratic upstream interpolation, Comp. Meth. in Appl. Mech. Engng. 19 (1979) 59-78.

[18] S. V. Patankar, Numerical Heat Transfer and Fluid Flow, Hemisphere Publ. Co., Washington, DC, 1980.

[19] S. V. Patankar, Recent developments in computational heat transfer, J. Heat Transfer 110 (1988) 1037-1045.

[20] M. Corcione, E. Habib, Bouyant heat transport in fluids across tilted square cavities discretely heated at one side, Int. J. Therm. Sci. 49 (2010) 797-808